Vibrational Spectroscopy and Structural Analysis of $V^+(C_2H_6)_n$ Clusters ($n = 1 – 4$)

Jesse C. Marcum[a)] and Ricardo B. Metz[b)*]

a) Department of Chemistry, Keene State College, Keene, New Hampshire 03435, United States

b) Department of Chemistry, University of Massachusetts, Amherst, Amherst, Massachusetts 01003, United States

Abstract

The vibrational structure and binding motifs of vanadium cation-ethane clusters, $V^+(C_2H_6)_n$, for $n = 1 – 4$ are probed using infrared photodissociation spectroscopy in the C-H stretching region (2550 – 3100 cm^{-1}). Comparison of spectra to scaled harmonic frequency spectra obtained using density functional theory suggest that ethane exhibits two primary binding motifs when interacting with the vanadium cation, an end-on η^2 configuration and a side-on configuration. Determining the denticity of the side on isomer is complicated by the rotational motion of ethane, implying that structural analysis based solely on Born-Oppenheimer potential energy surface minimizations is insufficient, and that a more sophisticated vibrationally adiabatic approach is necessary to interpret spectra. The lower-energy side-on configuration predominates in smaller clusters, but the end-on configuration becomes important for larger clusters as it helps to maintain a roughly square planar geometry about the central vanadium. Proximate C-H bonds exhibit elongation and large red-shifts when compared to bare ethane, particularly in the case of the side-on isomer, which are underestimated by scaled harmonic frequency calculations, demonstrating initial effects of C-H bond activation. Tagging several of the clusters with argon and nitrogen results in non-trivial effects. The high binding energy of N_2 can lead to the displacement of ethane from a side-on configuration into an end-on configuration. The presence of either one or two Ar or N_2 can impact the overall symmetry of the cluster, which can alter the potential energy surface for ethane rotation in the side-on isomer and may affect the accessibility of low-lying electronic excited states of V^+.

*Author to whom correspondence should be addressed: Email: rbmetz@chem.umass.edu; Phone: +1-413-545-6089; Fax: +1-413-545-4490

Introduction

The activation of hydrocarbon bonds has enjoyed considerable study over the last several decades.[1,2] Such studies have become more important recently along with an increased global reliance on natural gas, which is largely composed of simple hydrocarbon compounds such as methane and ethane.[3] Although natural gas is widely used as an energy source, much of its potential for use is left unrealized due to the lack of chemical functionality.[4] Expanding the chemical functionality of constituent compounds such as ethane and methane generally involves some form of C-H or C-C bond activation as an early step.[5]

A large and growing body of work has focused on studying how transition metals can be used to induce bond activation and thus catalyze functionalization reactions.[2] Much of this work has focused on bond activation in methane, in large part due to its high concentration in natural gas and its experimentally tractable size.[6–8] While the smaller size of methane may make it more attractive for in-depth study of C-H bond activation, ethane is the smallest hydrocarbon in which C-C bond activation can also occur. Ethane thus has a greater number of possible reactive pathways when interacting with transition metal species,[6–13] which should contribute to its potential as a chemical feedstock.

The use of solid-state or surface-based transition metal catalysis is widespread in industry, but it is also possible to catalyze hydrocarbon functionalization using small clusters.[1,14] Such cluster studies are not only a means of catalysis, but can also serve as experimentally tractable models for understanding catalysis in larger systems. When hydrocarbons interact with individual transition metal atoms and ions, as well as small clusters of atoms, the resulting chemistry can be similar to what occurs at surface defects in bulk systems.[1,15–20]

A number of studies have investigated the ability of the vanadium cation to activate hydrocarbon bonds.[12,14,21–24] Work by Armentrout and coworkers investigated the ability of V^+ to induce reactions with methane,[14] ethane,[12] and propane[22] in guided ion beam studies. In all studies, V^+ was found to be more reactive in the excited triplet state than when in the quintet ground state, implying lower barriers on the triplet potential energy surface, which is accessed via electronic excitation of the reactant or intersystem crossing during the course of the reaction. Zhang and Feng[24] calculated C-H and C-C activation of ethane by V^+, but they did not map the potential energy surfaces for both spin states. We have done so, and the results are shown in Figures S1 and S2. Although the lowest energy product of C-H activation is quintet $V^+(C_2H_4) + H_2$, the key intermediates and rate-determining barriers on the minimum energy path are triplets. For C-C activation, the key intermediates and $VCH_2^+ + CH_4$ product are triplets. The C-C activation pathways have higher barriers than for C-H activation, and the products are substantially more endothermic. This energetic preference for low-spin reaction intermediates is a consistent theme in reactions between alkanes and M^+ ions for many different metals. In the case of ethane, a number of

reactions were observed, with the most prevalent being symmetric cleavage of the C-C bond to form VCH_3^+ and CH_3 and cleavage of a C-H bond to form VH^+ and C_2H_5. Both of these channels were found to be endothermic with the C-C bond cleavage reaction being the lowest energy reaction of all those observed. Although dehydrogenation was observed to be exothermic, the process was found to be inefficient. Our calculations predict a large, 95.4 kJ/mol, activation barrier on the quintet surface, or a 32.2 kJ/mol barrier on the triplet surface, which would require intersystem crossing during the course of the reaction. Later experiments by Weisshaar and coworkers,[25–27] and very recently by Ng, Armentrout, and coworkers,[28] using state selected ion beams observed much higher reactivity for triplet than quintet states in the dehydrogenation of ethane. As shown in Figure S1, triplet V^+ should readily dehydrogenate ethane, as it has the proper spin and sufficient energy to overcome all barriers to produce triplet or quintet $V^+(C_2H_4) + H_2$. While these studies reveal the importance of the triplet excited state of V^+, understanding how the quintet ground state interacts with ethane is also important because it serves as an entrance channel to reactive pathways.[29,30] Even in these less-reactive entrance channels, metal cations can induce substantial red-shifts in C-H stretching modes,[21] which must be accurately accounted for in order to generate reliable potential energy surfaces for activation pathways. It is therefore important to understand the structural details of such entrance channel complexes and determine the specific nature by which V^+ influences bound ethanes.

In this paper, we report vibrational spectra of vanadium-ethane clusters, $V^+(C_2H_6)_n$ for $n = 1 – 4$, obtained using photodissociation spectroscopy. These spectra, accompanied by computational chemistry calculations, are used to identify important cluster binding motifs and determine ways in which V^+ affects the C-H and C-C bonds in ethane.

Methods

Experimental

Experimental infrared photodissociation spectra are obtained using home-built instrumentation consisting of a laser ablation source, a dual-stage reflectron time-of-flight mass spectrometer, and a tunable infrared laser source. Details of the experimental setup are described elsewhere,[30,31] so only a brief description is provided here, with additional detail in Supporting Information.

Both tagged and untagged $V^+(C_2H_6)_n$ clusters are produced by laser ablation of a vanadium rod, followed by clustering with ethane, diluted in $He/Ar/N_2$, introduced via pulsed valves.[32] Cluster ions cool as they expand into vacuum, forming a molecular beam that is skimmed before entering the acceleration region of a two-stage time-of-flight mass spectrometer. Prior experiments using the same source suggest that clusters are formed with a rotational temperature of ca. 15 K, and a vibrational temperature that is likely higher.[33] Ions are accelerated into the first stage of the mass spectrometer and are mass selected by

the time they reach the turning point of a reflectron where a multi-pass mirror arrangement[34] is used to irradiate cluster ions of interest using the output of a Nd:YAG-pumped OPO/OPA system that is tunable from 2500-4000 cm^{-1}, is capable of generating ~5 mJ/pulse near 3000 cm^{-1}, and has a line width of ~1.8 cm^{-1}. Fragment ions produced as the result of laser irradiation and dissociation, as well as any undissociated parent ions, are reaccelerated by the reflectron and enter the second stage of the mass spectrometer where they are mass-analyzed and detected. Photodissociation spectra are obtained by monitoring the ratio of fragment to parent ion signal, normalized to laser power, as a function of the laser wavenumber.

Depending on the cluster being studied, the binding energy of ethane to vanadium may be too large to induce dissociation of the cluster using the photon energies available in our experiment. In such cases, where clusters of interest result in either no dissociation or extremely low dissociation, we employ the tagging method. During expansion and cooling in the cluster source, it is possible for some of the carrier gas (either argon atoms or nitrogen molecules in this experiment) to become weakly bound as part of the ionic cluster. Upon absorption of infrared radiation, tagged versions of clusters may undergo dissociation by loss of the weakly bound argon atom(s) or nitrogen molecule(s). Ideally, the geometry of the molecular clusters is only weakly perturbed by the presence of a tag; however, it is possible for tagging to result in a change in cluster geometry in certain cases.

Computational

Quantum chemical computations employing density functional theory are used to determine geometric isomers, energies, and theoretical vibrational spectra of each cluster species. All computations are performed using the Gaussian 09 suite of programs.[35] Following exploratory computations with different multiplicities, all subsequent computations consider only quintet states due to the large quintet-triplet energy gap ($\gtrsim$ 6000 cm^{-1} for equilibrium geometries). Computations primarily utilize the B3LYP density functional,[36] although the addition of empirical dispersion[37] and the M11L density functional[38] are also used for exploratory calculations and to verify that the choice of functional does not have a large influence on predicted structure and properties. Unless otherwise noted, computational results refer to B3LYP calculations using 6-311++G(3df,3pd) basis set. To compensate for the over-estimation of vibrational frequencies when performing harmonic frequency analysis, vibrational frequencies are scaled by a factor of 0.966, which is obtained by comparing computational results for the various C-H stretching frequencies of ethane to experimental values.[39,40] Stick spectra from scaled-harmonic frequency calculations are convolved with a Gaussian function corresponding to a spectral resolution of 20 cm^{-1} to produce simulated vibrational spectra of optimized geometries. Unscaled harmonic frequencies are used

to determine zero-point energy corrections for all optimized geometries, and scaled harmonic frequencies are used to determine zero-point contributions to vibrationally adiabatic potential energy surfaces.

Results and Discussion

General Isomer Classes and Overview of Spectra

Prior to discussing experimental results, it is useful to consider the two major classes of $V^+(C_2H_6)$ isomers identified during computational work. These two isomer classes are not only important for interpreting the photodissociation spectra of the various tagged $V^+(C_2H_6)$ clusters, but they also form the basis for understanding the larger clusters. Structures of the two primary isomer classes are presented in Figure 1, which we term "end-on" and "side-on". In both side-on and end-on isomer classes, ethane adopts a staggered geometry.

In the case of the end-on isomer, ethane binds to the vanadium cation with η^2 denticity, where two hydrogen atoms—both attached to the same carbon atom—point toward vanadium. This end-on configuration is structurally similar to the configuration adopted by methane when binding to the vanadium cation.[21]

In the case of the side-on isomer, vanadium interacts with hydrogen atoms that are connected to the different carbon atoms. Although Figure 1 depicts the side-on isomer as having an overall denticity of η^2, determining the actual denticity is not straightforward. The actual denticity is connected to the hindered rotor motion of the ethane about the C-C bond axis and is a major focus of the discussion below.

A summary of binding energies for all $V^+(C_2H_6)_n$ clusters, including these two isomer classes, is given in Table 1. Geometries, energies, and harmonic frequencies/intensities are included in Supporting Information. In the case of $V^+(C_2H_6)$, computational results predict the side-on isomer to be the lowest energy isomer class, being ca. 1100 cm^{-1} lower in energy than the end-on isomer. For the side-on isomer of $V^+(C_2H_6)$, ethane is calculated to have a binding energy of 7760 cm^{-1}.

Figure 2 depicts experimental photodissociation spectra for $V^+(C_2H_6)_n$ clusters (n = 1 – 4), some of which were obtained using argon or nitrogen tagging. Corresponding peak positions are included in Supporting Information, Table S1. All spectra can be divided into two main regions: one above and one below 2855 cm^{-1}. Regardless of isomer, computational results indicate that features below 2855 cm^{-1} are due to stretching modes of C-H bonds proximate to the vanadium cation, while features above 2855 cm^{-1} are due to stretching modes of distal C-H bonds. In this paper, all features are compared to C-H stretching frequencies of bare ethane, which occur at 2896 cm^{-1} (a_{2u}), 2954 cm^{-1} (a_{1g}), 2969 cm^{-1} (e_g) and 2985 cm^{-1} (e_u).[40] The red-shift of proximate C-H stretching modes in comparison to the stretching modes of bare ethane is consistent with prior experiments on metal-methane clusters, and can be explained by a shift in electron density from C-H bonding orbitals to empty or partially empty metal orbitals and back-donation

from the metal into C-H anti-bonding orbitals.[30] Peaks in the region above 2855 cm^{-1} due to distal C-H stretching modes are clustered around where one would expect to see a free-CH stretch.[21,41] This is consistent with a decoupling of proximate and distal C-H bonds that would be expected as compared to bare ethane.

Perhaps the most important trend to note is the marked shift in overall peak structure that occurs between the untagged and nitrogen-tagged versions of $V^+(C_2H_6)_2$. The spectra of all $V^+(C_2H_6)$ clusters and the untagged $V^+(C_2H_6)_2$ cluster exhibit prominent peaks in the region below 2855 cm^{-1} and a conspicuous absence of resolved peaks in the region above 2855 cm^{-1}. These peaks below 2855 cm^{-1} are generally broad or have a high-energy shoulder.

In contrast, the spectra for the nitrogen-tagged species $V^+(C_2H_6)_2(N_2)$, for $V^+(C_2H_6)_3$, and for $V^+(C_2H_6)_4$ all exhibit well-resolved peaks above 2855 cm^{-1}. Furthermore, the prominent features below 2855 cm^{-1} do not appear to have high-energy shoulders; rather, they either exhibit a low-energy shoulder or consist of several resolved peaks where the low-energy peak has the smaller amplitude.

This marked shift in overall peak structure implies a corresponding shift in binding motif, or at least a change in the relative importance of different possible binding motifs. As will be discussed below, we attribute this shift to a change in the relative importance of the side-on vs. end-on isomers. In the case of all $V^+(C_2H_6)$ clusters and the untagged $V^+(C_2H_6)_2$ cluster, we find that the side-on isomer predominates and that the end-on isomer is of little importance. As cluster size grows and the available space for coordination with vanadium decreases, the end-on isomer becomes more important.

Finally, we note a clearly non-zero baseline that occurs in the spectra of $V^+(C_2H_6)(N_2)$ and $V^+(C_2H_6)(Ar)$ that does not occur in any other spectrum. As will be described below, this observation can be explained by considering the accessibility of low-lying electronic transitions.

$V^+(C_2H_6)$

Figure 3 depicts experimental photodissociation spectra for $V^+(C_2H_6)$, each obtained using a different tagging method. Although we were able to produce untagged $V^+(C_2H_6)$, we were unable to detect any photodissociation. As mentioned above, the binding energy of the side-on isomer is calculated to be 7760 cm^{-1} using the B3LYP functional. This energy is well beyond the spectral range of our experiment—requiring the absorption of at least three photons to induce dissociation—so we instead used the tagging method. Ideally, tagging does not perturb the structure or spectrum strongly, but can sometimes lead to important effects. Calculated binding energies for argon-tagged species using the B3LYP functional are 2525 cm^{-1} for the first argon atom, and 1721 cm^{-1} for a second. These binding energies, which are consistent with prior studies,[42,43] are both within our experimental spectral range, allowing for the possibility of single-photon dissociation at all wavelengths. This is not the case when

using nitrogen as a tagging species where the binding energy is calculated to be 6712 cm^{-1} for the first nitrogen and 5902 cm^{-1} for the second (when an ethane is also attached to V^+). When nitrogen is used as a tagging species, spectra can only be produced by infrared multiple-photon dissociation (IRMPD).

The lower binding energies of tagged species generally result in colder temperatures in comparison to untagged clusters. The main, low-energy feature in the experimental spectra is narrower for clusters tagged with two argon atoms as compared when the cluster is tagged with a single argon atom. The nitrogen-tagged clusters exhibit similar behavior. Furthermore, features in the nitrogen-tagged clusters are broader than those in the argon-tagged clusters. This is at least in part due to the significantly higher binding energy of nitrogen as compared to argon, which should cause both higher cluster temperatures, and the broadening typical of IRMPD.[44]

Tagging also results in modest shifts to spectral features. Addition of a second tag decreases the red shift of the primary spectral feature by ca. 20 cm^{-1} when using both argon and nitrogen. Additional bound species can serve as a dielectric by lending electron density to the vanadium cation, thereby reducing vanadium's charge and ability to polarize other species. In the present case, the reduced polarization of ethane leads to a decreased red-shift for the proximate C-H bonds. This is further corroborated by the fact that the proximate C-H bonds in nitrogen-tagged clusters exhibit even smaller red-shifts than the argon-tagged clusters. Nitrogen has a slightly larger polarizability than argon[45] and is oriented such that a terminal lone pair is directed toward vanadium, allowing for a stronger bond with vanadium, likely with some covalent character.[46] Simulated spectra from scaled harmonic frequency calculations exhibit similar behavior, where the first tag decreases the red-shift of modes involving proximate C-H stretches by 10-15 cm^{-1}, and the second decreases the shift by an additional 10-15 cm^{-1}. Based on this rough trend, we estimate that the lowest-energy C-H stretch of untagged $V^+(C_2H_6)$ should occur near 2620 cm^{-1}. This corresponds to a redshift of ca. 276 cm^{-1} compared to the lowest-energy C-H stretch in bare ethane. This is substantially larger than the redshift experienced by methane in $V^+(CH_4)$, which is estimated to be ca. 175 cm^{-1}.[21]

Immediately below experimental spectra in Figure 3 are scaled harmonic frequency spectra for the two isomer classes (side-on and end-on) of the untagged species. Argon tagging has little effect on the calculated spectra, other than the decreased red-shifts mentioned above. Experimental spectra for the argon-tagged clusters are consistent with the lower-energy side-on isomer class (1a), although the high-energy shoulder at ca. 2700 cm^{-1} makes it hard to entirely rule out the presence of at least some of the end-on isomer class (1b), which could result from kinetic trapping during the cluster formation process. When in the side-on isomer, two limiting configurations are possible, based on the denticity of ethane. In the first case, ethane binds to vanadium with overall η^2 denticity, where each C-H bond is attached to a different carbon atom. Throughout the remainder of this paper, we refer to this side-on isomer (1ai) as

having $\eta^{(1+1)}$ denticity. The second case consists of ethane binding to vanadium with overall η^3 denticity, where two C-H bonds are attached to the one carbon and the third C-H bond is attached to the other carbon. We refer to this side-on isomer (1aii) as having $\eta^{(2+1)}$ denticity.

Regardless of which configuration is the global minimum, it may be possible to interconvert between the $\eta^{(1+1)}$ and $\eta^{(2+1)}$ configurations if the potential energy surface is sufficiently flat. The interconversion of the two configurations corresponds to the rotation of ethane, roughly about the C-C bond, which harmonic frequency calculations predict to be the lowest-energy vibrational mode in the untagged clusters. If the barrier to rotation is sufficiently low, this ethane rotor mode should be treated not as having a harmonic potential, but as having a periodic potential characteristic of a hindered rotor.[47–50] Such motion would not just lend slight variation to the orientation of each C-H bond, but the interconversion of the $\eta^{(1+1)}$ and $\eta^{(2+1)}$ isomers will lead to the complete exchange of proximate and distal designations. Such conformational flexibility could have a large impact on the associated spectral signatures of the cluster. Prior computational investigations identified the $\eta^{(1+1)}$ side-on isomer as being the global minimum cluster geometry, but it is unclear if the ethane rotor motion was considered.[24] Similar work on the closely related complex $Ti^+(C_2H_6)$ identified end-on η^3 and side-on $\eta^{(2+1)}$ isomers to be minima on the potential energy surface and the $\eta^{(1+1)}$ isomer to be a maximum.[51] That study, however, did not further explore the effect of ethane rotation.

To further investigate this hindered rotor motion of ethane, we performed several energy scans of one of the HCCV dihedral angles in the side-on isomer of untagged $V^+(C_2H_6)$ using both the B3LYP and M11L density functionals. Discussion of our analysis is initially framed using data from B3LYP calculations and followed by comments on how the analysis is affected by using data from M11L calculations.

Using the B3LYP functional, if the geometry of ethane is allowed to relax at each point during the scan, the barrier height of rotation is calculated to be 145 cm^{-1} without incorporating zero-point energy and decreases to 33 cm^{-1} when adding in the zero-point energy of all other (i.e., non-rotor) modes. (Potential energy surfaces for ethane rotor motion are depicted in Figures S3 and S4.) Note that the rotational coordinate is defined such that 0° corresponds to a conformation with $\eta^{(2+1)}$ denticity. On this B3LYP potential energy surface of untagged $V^+(C_2H_6)$, minima correspond to structures with $\eta^{(1+1)}$ denticity (isomer 1ai), and maxima correspond to structures with $\eta^{(2+1)}$ denticity (isomer 1aii).

Presuming an experimental cluster temperature on the order of 50 K, the extremely low barrier to rotation in comparison to the amount of thermal energy available in our experiment ($k_BT \approx 35$ cm^{-1}) suggests that both the $\eta^{(1+1)}$ and $\eta^{(2+1)}$ configurations should be considered when interpreting experimental spectra. Simulated spectra for the C-H stretching region at representative HCCV dihedral angles are depicted in Figure 4. These spectra reveal the large peak shifts that occur as the proximate and distal

designations of C-H bonds undergo exchange upon rotation. They also reveal how the different symmetries of each rotational isomer lead to variability in how the C-H bonds couple to form normal modes. Points on the potential energy surface with the highest symmetry act as limiting cases for spectral interpretation. These points consist of the side-on isomers with $\eta^{(1+1)}$ denticity, which belong to the C_2 symmetry point group, and the side-on isomers with $\eta^{(2+1)}$ denticity, which have C_s symmetry. At all other points the cluster has C_1 symmetry, so interpretation of the associated normal modes is not as straightforward. Assignment of features for the two highest-symmetry cases is provided in Figure 4. We acknowledge that a more robust assignment of spectral features could likely be attained using permutation-inversion symmetry groups; however, such an analysis is beyond the scope of the present work. All features below 2855 cm^{-1} correspond to stretching modes of C-H bonds proximate to V^+, and those above 2855 cm^{-1} correspond to distal stretching modes. Peaks corresponding to distal bonds have much lower intensity than those corresponding to proximate bonds, which is in agreement with prior experiments where the presence of a metal cation was found to polarize proximate C-H bonds to make them stronger IR chromophores than typical C-H bonds.[41] Note that all computational spectra underestimate the red-shift of the proximate C-H stretching modes, regardless of rotational isomer. This is the case when using both the B3LYP and M11L density functionals, and even when empirical dispersion is included using Grimme's D3 approach.[37]

To understand how the hindered rotor potential energy surface influences the prevalence of the $\eta^{(2+1)}$ and $\eta^{(1+1)}$ configurations it is helpful to consider the associated wavefunctions and probability densities. We treat the hindered rotor motion separately from all other modes using a vibrationally adiabatic approach.[52–54] We justify this approach by pointing out that the unscaled harmonic frequency of the rotor mode is on the order of 50-80 cm^{-1}, whereas all other modes have unscaled harmonic frequencies of at least 250 cm^{-1}. Consequently, the timescale for rotor mode should be far longer than all other modes, causing it to be largely decoupled from all other vibrational motions. As the slow rotor motion occurs, all other modes should be able to "adapt" quasi-instantaneously to their respective new equilibrium positions. Briefly, our approach involves computing a weighted average of scaled-harmonic spectra of conformations along the hindered rotor coordinate. The weighting factors are determined using the probability densities of the hindered rotor wavefunctions, which are determined using the matrix formalism of perturbation theory.[47,48,50] A more detailed description of our approach is included in Supporting Information. Several spectra simulated using this approach are shown in Figure 3.

While the simulated spectra constructed using our rotor model do not achieve quantitative accuracy, they do help to explain the general shape of the $V^+(C_2H_6)$ experimental spectra. First, as the side-on ethane undergoes rotation and different C-H bonds come into and go out of alignment with V^+, the degree of red-shift associated with proximate C-H bonds undergoes a drastic change from 2660 to

2885 cm^{-1}. This change in frequency is accompanied by a change in intensity. This behavior can help explain the general breadth of the low-energy feature in $V^+(C_2H_6)$ experimental spectra, as well as the high-energy shoulder that is most notable in the spectrum of $V^+(C_2H_6)(Ar)_2$. Our model also helps to explain why peaks corresponding to distal C-H bonds are not observed in the experimental spectra. These modes undergo modest shifts upon ethane rotation and do not constructively combine to the same extent as the modes associated with proximate C-H bonds. The resulting broadening suppresses the overall intensity of the distal C-H peaks relative to the proximate C-H peaks (as compared to individual harmonic frequency spectra), making it more difficult to observe well-defined peaks given the signal-to-noise ratio in experimental spectra.

Our model is mildly sensitive to the input parameters (e.g., the height of the barrier, the rotational constant of ethane, etc.); however, this sensitivity affects the quantitative aspects of the simulated spectra and not the qualitative aspects. The simulated spectra presented in Figure 3 were generated using a temperature of T = 50 K and several sets of hindered rotor PES parameters (i.e., the barrier height and the rotational angle corresponding to the PES minimum) to explore differences in computational results obtained using B3LYP and M11L density functionals. Whereas the B3LYP surface has the $\eta^{(1+1)}$ structure as a minimum and a vibrationally adiabatic barrier height of 33 cm^{-1}, the M11L surface has the $\eta^{(2+1)}$ structure at a minimum and a 140 cm^{-1} barrier height. Despite the differences in PES parameters, the resulting simulated spectra exhibit remarkable similarity. This can be explained by considering the probability densities of the hindered rotor wavefunctions (Figure S5). Because of the low rotational barrier and generally flat PES, probability densities are not highly localized to PES minima but are instead broadly distributed over all rotational angles. Furthermore, except for a small number of eigenstates, probability densities are non-zero for all angles. All of this taken together, it is difficult to unequivocally determine the specific geometry of the lowest-energy side-on isomer. Rather, it is more prudent to consider the side-on ethane structure as existing in a hindered rotor state where all possible rotational isomers are, at least to some extent, present in the cluster. A more-detailed characterization of the hindered rotor PES would require more sophisticated and comprehensive computational and experimental methods.

The above analysis of $V^+(C_2H_6)$, including ethane rotor motion, is based on computations for the untagged cluster. Because our experimental spectra utilize the tagging method, it is important to consider how tagging may impact cluster geometry and spectra. The lowest-energy isomers (on the Born-Oppenheimer surface) for tagged $V^+(C_2H_6)$ are shown in Figure 5. In each of these clusters, vanadium binds in a roughly square-planar geometry, where each tag occupies one coordination site and the side-on ethane occupies two coordination sites. The presence of a tag perturbs the ethane rotor potential energy surface such that determining the denticity of ethane is even less straightforward than when untagged.

Whether the global minimum corresponds to $\eta^{(1+1)}$ or $\eta^{(2+1)}$ denticity depends on whether or not zero-point energy is included, whether the species is singly or doubly tagged, and the identity of the tagging species (see Figure S4). In the most extreme case, the presence of a single tag results in a three-fold periodic surface, in contrast to the six-fold periodic potential of bare and doubly tagged $V^+(C_2H_6)$. This represents a rare case where using fewer tags perturbs the cluster more than when using more tags. In all cases, however, the barrier to rotation remains low enough for probability densities to be broad and delocalized over all rotor angles, regardless of whether or not a tag is present.

A final feature to note is the clearly non-zero baseline that occurs in the spectrum of $V^+(C_2H_6)$ when tagged with either a single argon atom or single nitrogen molecule, but not when tagged with two argon atoms or two nitrogen molecules. Similar effects have been seen in vibrational spectra of $V^+(CH_4)_x(Ar)_y$ clusters, where a non-zero baseline is present in some clusters, but not others.[21] This effect can be explained on the basis of the cluster symmetry. When doubly tagged, the cluster has either C_s or C_2 symmetry, depending on whether the side-on ethane is in an $\eta^{(2+1)}$ or $\eta^{(1+1)}$ configuration. If the hindered rotor motion of the side-on ethane is taken into consideration by presuming a time-averaged configuration, the doubly tagged cluster would then have even higher C_{2v} symmetry. With only a single tag, however, only three of the four square-planar coordination sites are occupied. Consequently, the highest order symmetry point group to which the cluster could belong is C_s, even if ethane is considered in a time-averaged rotational configuration. If there exist any low-lying excited electronic states of $V^+(C_2H_6)$ that are spectroscopically inaccessible due to symmetry related selection rules, the presence of a single tag could reduce the symmetry of the cluster such that these transitions become symmetry allowed. A doubly tagged cluster, however, would belong to a higher-order symmetry point group where the transitions remain symmetry forbidden. One possible candidate for such a transition could be between the ^5D ($3d^4$) electronic ground state and the ^5F ($3d^3 4s$) first electronic excited state.[22,55] This transition is Laporte forbidden for the bare atom, but it could become symmetry allowed when ligands are present in an appropriate geometry. Furthermore, these states are separated by 2470 – 2825 cm^{-1} for the bare atom (depending on the spin-orbit levels involved), which lies within our experimental range. Alternatively, a reduction in the symmetry of the cluster could affect the *d*-orbital splitting of vanadium, lowering the energy of an excited electronic state into a range accessible in our experiment.

$V^+(C_2H_6)_2$

One of the largest peaks observed in most of our mass spectra corresponds to untagged $V^+(C_2H_6)_2$ (see Figure S7). This was the case for a wide variety of source settings and conditions, indicating that the cluster is particularly stable and that $n = 2$ might constitute a "magic number".[56] Though we did not observe argon-tagged versions of this cluster, we were able to form a nitrogen-tagged version. The

photodissociation spectrum of untagged $V^+(C_2H_6)_2$ is depicted in Figure 6, and that of the tagged version, $V^+(C_2H_6)_2(N_2)$, is depicted in Figure 7. The spectrum of $V^+(C_2H_6)_2$ is remarkably similar to that of $V^+(C_2H_6)$—especially the double-tagged versions—whereas the nitrogen-tagged version is more similar to the spectra of clusters with $n = 3 – 4$ (see Figure 2). Geometry optimizations using the B3LYP functional indicate several isomer classes, the lowest of which has two ethanes in a side-on configuration and overall geometry that is roughly square planar (2a). Low-energy isomers are shown in Figure 6, and their associated energies are listed in Table 1.

In the lowest-energy class, several isomers are based on the denticity and relative orientation of the two side-on ethane molecules. Potential energy surface scans reveal that the hindered rotor motions of the two ethane molecules are weakly coupled by ca. 30 cm^{-1} (see Figure S8). In this limit of weak interaction, the vibrational spectrum would be expected to be nearly identical to that of $V^+(C_2H_6)$, aside from a decreased red-shift of the proximate C-H bonds. This is largely consistent with the observed spectrum, aside from the more pronounced shoulder at ca. 2700 cm^{-1} in the spectrum of $V^+(C_2H_6)_2$. This more pronounced shoulder likely arises from either the hindered rotor motion of the two ethane molecules (see above) or due to the presence of other isomers that include end-on configurations of ethane. Higher energy isomer classes consist of either one side-on and one end-on ethane (2b, which is 892 cm^{-1} higher), or two end-on ethanes (2c, which is at least 1747 cm^{-1} higher). These higher energy isomer classes are only expected to be present in our experiment if they become kinetically trapped during the expansion and cooling process.

In principle, the hindered rotor analysis described above could also be extended to the case of $V^+(C_2H_6)_2$. The coupling of the two ethanes would result in a non-separable Hamiltonian, and such a treatment is beyond the scope of this study. In general, however, the same ideas from the hindered rotor analysis should also apply here. The low barrier to ethane rotation in the side-on isomer should result in a broadening of peaks as the alignment of C-H bonds toward vanadium undergoes changes and the proximate and distal designations undergo exchange. Similar to the case of $V^+(C_2H_6)$, we believe it prudent to consider the geometry of untagged $V^+(C_2H_6)_2$ as consisting of two side-on ethanes existing in hindered rotor states where all rotational isomers are simultaneously present.

The spectrum of $V^+(C_2H_6)_2(N_2)$ in Figure 7 is markedly different than that of untagged $V^+(C_2H_6)_2$, indicating different ethane binding motifs. In the lowest-energy isomer class, both ethanes and the nitrogen are predicted to bind to vanadium in a roughly square planar structure, as was the case for the other clusters discussed so far. This isomer class consists of one side-on ethane, one end-on ethane, and nitrogen binding to vanadium with η^1 denticity. The side-on ethane occupies two coordination sites, as above, but the end-on ethane appears to occupy only a single coordination site, despite having η^2 denticity.

Here, the binding energy of nitrogen to vanadium is very similar to the binding energy of ethane to vanadium when in the side-on configuration (both are ca. 7000 cm^{-1}, depending on the cluster). This allows nitrogen to compete with ethane as a ligand. Even when considering roughly square-pyramidal geometries with two side-on ethanes bound in a roughly square-plane and nitrogen bound along the *z*-axis, geometry optimizations converged to the fully square-planar minimum-energy isomer. Instead of completely displacing ethane from the cluster, the nitrogen forces one ethane molecule to adopt the higher-energy end-on configuration, thus preserving the roughly square-planar geometry. Within this isomer class are two different isomers, separated by 29 cm^{-1}, where the end-on ethane is oriented roughly parallel to either the side-on ethane or the N_2 molecule. Both simulated spectra exhibit similar agreement with the experimental spectrum, and both cluster geometries are likely to be present in our experiment.

Based on comparison to $V^+(C_2H_6)$ clusters, the peak observed at 2640 cm^{-1} in the spectrum of $V^+(C_2H_6)_2(N_2)$ likely corresponds to C-H stretching modes of the side-on isomer. The peak at 2705 cm^{-1} is likely due to the symmetric stretch of the proximate CH_2 group in the end-on ethane, with the high-energy shoulder at ca. 2760 cm^{-1} being due to the anti-symmetric stretch. As was the case for $V^+(C_2H_6)$ clusters, the scaled harmonic frequency calculations continue to underestimate the red-shift of proximate C-H stretching modes in the side-on isomer, but the predicted red-shifts of proximate C-H stretches of the end-on isomer are more reasonable. The peaks at 2956 and 2999 cm^{-1} in the experimental spectrum are likely due to modes involving distal C-H stretches of the end-on ethane, as opposed to the side-on ethane, as distal stretches from side-on ethane are likely too weak to be observed in our experiment (see above). This is corroborated by scaled harmonic frequency spectra, where distal C-H stretches of end-on ethane have oscillator strengths that are, on average, ca. ten times higher than those associated with side-on ethane.

$V^+(C_2H_6)_3$

The photodissociation spectrum of $V^+(C_2H_6)_3$ (Figure 2 and Figure 8) is remarkably similar to that of $V^+(C_2H_6)_2(N_2)$, but with better-resolved features, implying similar binding motifs for the clusters. Features in the high-energy region above 2855 cm^{-1} do not experience a discernable shift (Figure 2), but features below 2855 cm^{-1} occur at higher energies, consistent with decreased red-shifts when more polarizable groups are present in the cluster. Equilibrium geometries of clusters can again be divided into several classes based on the number of side-on and end-on ethanes in the cluster (Table 1). The lowest-energy class (3a) consists of one side-on and two end-on ethanes, all within 125 cm^{-1}. All isomers in classes 3a and 3b appear to be roughly square planar, with side-on ethanes occupying two coordination sites and end-on ethanes occupying a single binding site (again, despite having η^2 denticity). Isomer class 3c does involve two ethanes in the more stable side-on configuration, but the third ethane can only bind in

an end-on η^1 configuration along the *z*-axis of the square plane (Table 1). The energetic cost associated with displacing a side-on ethane into an end-on configuration is apparently outweighed by the tendency for vanadium to maintain a roughly square planar configuration. This observation is in line with prior studies that note the tendency for V^+ to support a coordination number of four in a square planar configuration.[12,43,46]

Despite the variability in the specific positioning of the end-on ethanes in this isomer class, their simulated spectra are remarkably similar. The peak that appears at ca. 2710 cm^{-1} in the simulated spectra is largely due to proximate C-H stretches of the side-on ethane, and likely corresponds to the experimental peak at ca. 2650 cm^{-1}, based on comparison to the spectra of smaller clusters. Peaks at ca. 2750 cm^{-1} and ca. 2808 cm^{-1} in the simulated spectra are due to proximate C-H stretches of end-on ethanes, and likely correspond to experimental peaks at 2710 and 2780 cm^{-1}, respectively. The peaks at 2650 cm^{-1} and 2710 cm^{-1} exhibit a larger difference in relative intensity than do the analogous peaks in the spectrum of $V^+(C_2H_6)_2(N_2)$, which is likely due to the presence of more end-on isomers in the cluster.

If these assignments are accurate, then scaled harmonic frequency calculations using the B3LYP functional underestimate the red-shift of proximate C-H stretching modes to a larger extent for larger cluster sizes. Including empirical dispersion in the computations using Grimme's D3 approach leads to a slight improvement by 2 – 10 cm^{-1}, but this is not nearly enough to account for the ca. 40 – 60 cm^{-1} difference that we observe.

As was the case for $V^+(C_2H_6)_2(N_2)$, the higher-energy features above 2855 cm^{-1} are likely due to distal C-H stretching modes of ethanes in the end-on conformation. Although the side-on isomer should also have modes in this region, they are substantially weaker and not likely to be observed given our experimental signal-to-noise ratio. Whereas the distal C-H stretching modes of end-on ethanes all combine to form two main spectral features in the simulated spectra at ca. 2950 and 3015 cm^{-1}, the experimental spectrum exhibits several more well-defined peaks. We are unable to make specific assignments to each of these peaks without further information.

$V^+(C_2H_6)_4$

The photodissociation spectrum of $V^+(C_2H_6)_4$ is shown in Figure 9 along with structures for the lowest-energy isomer class, 4a. The similarity to the spectra of $V^+(C_2H_6)_2(N_2)$ and $V^+(C_2H_6)_3$ again indicates similar binding motifs. The poorer signal-to-noise ratio reflects the very small quantities of $V^+(C_2H_6)_4$ that can be made in our experiment. High-energy features above 2855 cm^{-1} again do not experience a discernable shift but features below 2855 cm^{-1} occur at higher energies, consistent with decreased red-shifts as cluster size and polarizability grow (Figure 2). Isomer classes are again based on the number of ethanes in side-on vs. end-on configurations; however, it is not possible to maintain the

roughly square planar configuration about a central vanadium unless all four ethane molecules are in the end-on configuration. The tendency for vanadium to bind in a square planar configuration continues to outweigh the energetic cost associated with displacing a side-on ethane into an end-on configuration. Consequently, the lowest-energy class of isomers (4a) has all four ethanes in the end-on configuration. The variation in relative position of the ethanes results in modest differences in energy (ca. 80 cm^{-1} for each pair of adjacent ethanes in a parallel, non-collinear arrangement), and virtually no difference in the associated spectra.

Spectral assignments for $V^+(C_2H_6)_4$ are largely the same as for $V^+(C_2H_6)_3$, albeit with one major difference; the lowest-energy isomer of $V^+(C_2H_6)_4$ does not include a side-on ethane and should therefore not exhibit an associated peak. The peak at 2647 cm^{-1} has a red-shift that is consistent with the side-on features observed in all smaller clusters, indicating the presence of at least some side-on isomer in the experiment. This also indicates that cluster formation involves some degree of kinetic trapping, at least under our experimental conditions. For example, if a cluster is formed by sequentially adding a fourth ethane to an already existing cluster of $V^+(C_2H_6)_3$ in the lowest-energy isomer class (3a), two possibilities arise. In one scenario, the fourth ethane displaces the side-on ethane into an end-on configuration so that the cluster can maintain a square planar geometry, resulting in one of the 4a isomers. This would result in a net binding energy of ca. 1485 – 1775 cm^{-1} for the fourth ethane, depending on the specific isomers involved (Table 1). In another scenario, the fourth ethane may adopt an end-on η^1 configuration along the *z*-axis of the square plane, resulting in one of the 4b isomers, which would maintain the original, underlying 3a structure of $V^+(C_2H_6)_3$. This would result in a net binding energy of ca. 290 – 296 cm^{-1} for the fourth ethane, depending on the specific isomers involved.

These ideas can be extended to infer the viability of larger clusters. Based on coordination number alone, it would be impossible for a cluster with five ethanes to exhibit square planar binding, meaning that at least one ethane would have to bind in an end-on η^1 configuration. If end-on η^1 ethanes are added to isomer 4ai to form a quasi-square pyramidal $V^+(C_2H_6)_5$ and a quasi-octahedral $V^+(C_2H_6)_6$, the binding energy is calculated to be 234 cm^{-1} for the fifth ethane and 175 cm^{-1} for the sixth.

Bond Activation

Given the above discussion of vibrational spectra and cluster structure, it is useful to consider how the presence of V^+ affects the C-H and C-C bonds in ethane and how these results compare to similar systems. The red-shift of proximate C-H bonds is generally indicative of bond weaking and is accompanied by elongation. For $V^+(C_2H_6)$, both the binding energy and the red shift exhibited by proximate C-H bonds in the side-on isomer is considerably larger than that observed in $V^+(CH_4)$

clusters.[21] The end-on isomer, however, has a red shift and binding energy that is closer to that of $V^+(CH_4)$, which is likely due to the similar η^2 binding motif.

Binding to V^+ results in elongation of the proximate C-H bonds by 2.0 – 2.3% for the end-on isomer and by 2.6% for the side-on isomer (when in the $\eta^{(1+1)}$ configuration). The calculated potential energy surface for the $V^+ + C_2H_6$ reaction (dashed lines in Figure S1) shows that the barrier for C-H activation starting from the end-on isomer is 10.6 kJ/mol lower than for the side-on isomer, as the initial energy is 12.8 kJ/mol higher and the energy of the transition state increases by only 2.2 kJ/mol. Furthermore, it is important to note that computations using the B3LYP/6-311++G(3df,3pd) level of theory underestimate the red-shift of proximate C-H bonds, especially in the case of the side-on isomer, indicating that studies based on B3LYP or M11L calculations alone may not accurately capture the extent to which C-H bond activation occurs.

Although we cannot directly probe C-C bond characteristics in our experiment, computations reveal that they are affected by the presence of V^+. The C-C bond length is calculated to change by negligible amounts for all isomers but the vibrational frequency associated with the C-C stretch decreases by 2.5% for only the side-on isomer. This indicates that the side-on isomer may have greater potential for C-C bond activation, which is generally in line with the mechanisms proposed for metal-initiated C-C bond cleavage in a number of systems.[1,10,24,51,57]

Conclusions

Photodissociation spectroscopy of vanadium cation-ethane clusters in the C-H stretching region in concert with computational results provides information about cluster binding motifs. Clusters exhibit a general tendency to bind in a square-planar geometry about vanadium when possible. Ethanes adopt either a side-on or end-on configuration based on the number of available binding sites. The lower-energy side-on isomer is expected to exhibit a mixture of both $\eta^{(1+1)}$ and $\eta^{(2+1)}$ denticity due to the low barrier to rotation about the C-C bond. The higher energy end-on isomer exhibits η^2 denticity when occupying a square planar binding site and is expected to exhibit η^1 denticity along the *z*-axis in larger clusters where all square planar sites are already occupied. Clusters' geometries are expected to be dominated by the lowest-energy isomer class for each cluster size, although we do observe evidence of possible kinetic trapping into higher-energy isomer classes for $V^+(C_2H_6)_4$.

Simulated scaled harmonic frequency spectra obtained using density functional theory are generally consistent with experimental spectra, although the red-shift of some proximate C-H stretching modes is underestimated and not all peaks observed in the experimental spectra can be accounted for. The large degree of spectral shifting—and consequent change in zero-point energy—that occurs upon ethane rotation in the side-on isomer highlights the importance of not relying solely on the Born-Oppenheimer

approximation when searching for geometries on extremely flat potential energy surfaces. The observed red-shift of proximate C-H bonds is greater than is observed in vanadium-methane clusters, particularly when ethane is in the side-on configuration, indicating a larger potential for C-H bond activation. Activation of the C-H bonds in ethane is thus expected to be greatest in smaller cluster size, where the side-on isomer is most prevalent and the interaction with V^+ is most direct.

Supporting Information

Potential energy surfaces for C-H and C-C bond activation (Figure S1 and Figure S2); Details of experimental and computational methods; Experimentally determined peak positions from photodissociation spectra (Table S1); Hindered rotor potential energy surfaces for tagged and untagged $V^+(C_2H_6)$ (Figures S3 and S4); Detailed assignment of features present in the scaled harmonic frequency spectra of $V^+(C_2H_6)$ when in a side-on configuration; Detailed description of hindered-rotor modeling, including probability densities for selected eigenstates (Figure S5) and vibrationally adiabatic spectral simulation steps (Figure S6); Sample mass spectrum of vanadium-ethane clusters (Figure S7); Two-dimensional potential energy surface for $V^+(C_2H_6)_2$ (Figure S8); A list of the energies, geometries, and unscaled harmonic vibrational frequencies and intensities of each isomer listed in manuscript Table 1, as well as for selected tagged clusters described in the manuscript (Table S2)

Acknowledgements

RBM gratefully acknowledges financial support from the National Science Foundation under award no. CHE-1856490. JCM gratefully acknowledges Framingham State University for funding the sabbatical during which the experimental portion of this work was conducted. JCM gratefully acknowledges Keene State College for providing start-up funds that were used in completing the theory and analysis portions of this work. Both authors are grateful for computational resources provided by the Massachusetts Green High-Performance Computing Cluster (MGHPCC).

Author Information

Corresponding Author

Ricardo B. Metz – Department of Chemistry, University of Massachusetts, Amherst, Amherst, Massachusetts 01003, United States; orcid.org/0000-0003-1933-058X;
Phone: +1-413-545-6089; Email: rbmetz@ chem.umass.edu; Fax: +1-413-545-4490.

Author

Jesse C. Marcum – Department of Chemistry, Keene State College, Keene, NH 03435, United States; orcid.org/0000-0001-6342-4263; Phone: +1-603-358-2568; Email: jesse.marcum@keene.edu.

Note

The authors declare no competing financial interest.

References

(1) Roithová, J.; Schröder, D. Selective Activation of Alkanes by Gas-Phase Metal Ions. *Chem. Rev.* **2010**, *110* (2), 1170–1211. https://doi.org/10.1021/cr900183p.

(2) Crabtree, R. H. Introduction to Selective Functionalization of C−H Bonds. *Chem. Rev.* **2010**, *110* (2), 575–575. https://doi.org/10.1021/cr900388d.

(3) Kidnay, A. J.; Parrish, W. R.; McCartney, D. G. *Fundamentals of Natural Gas Processing*, 3rd ed.; CRC Press: Boca Raton, 2019. https://doi.org/10.1201/9780429464942.

(4) Caballero, A.; Pérez, P. J. Methane as Raw Material in Synthetic Chemistry: The Final Frontier. *Chem. Soc. Rev.* **2013**, *42* (23), 8809–8820. https://doi.org/10.1039/C3CS60120J.

(5) Armentrout, P. B. Chemistry of Excited Electronic States. *Science* **1991**, *251* (4990), 175–179. https://doi.org/10.1126/science.251.4990.175.

(6) Sievers, M. R.; Chen, Y.-M.; Haynes, C. L.; Armentrout, P. B. Activation of CH_4, C_2H_6, and C_3H_8 by Gas-Phase Nb^+ and the Thermochemistry of Nb–Ligand Complexes. *Int. J. Mass Spectrom.* **2000**, *195–196*, 149–170. https://doi.org/10.1016/S1387-3806(99)00170-0.

(7) Georgiadis, R.; Armentrout, P. B. Reactions of Ground State Cr^+ with C_2H_6, C_2H_4, Cyclo-C_3H_6, and Cyclo-C_2H_4O: Bond Energies for $CrCH^+_n$ (n = 1–3). *Int. J. Mass Spectrom. Ion Process.* **1989**, *89* (2), 227–247. https://doi.org/10.1016/0168-1176(89)83062-9.

(8) Crabtree, R. H. Aspects of Methane Chemistry. *Chem. Rev.* **1995**, *95* (4), 987–1007. https://doi.org/10.1021/cr00036a005.

(9) Dobereiner, G. E.; Crabtree, R. H. Dehydrogenation as a Substrate-Activating Strategy in Homogeneous Transition-Metal Catalysis. *Chem. Rev.* **2010**, *110* (2), 681–703. https://doi.org/10.1021/cr900202j.

(10) Zhang, D.; Wang, R.; Zhu, R.; Zhang, D.; Wang, R.; Zhu, R. A New Pathway for Activation of C–C and C–H Bonds by Transition Metals in the Gas Phase. *Aust. J. Chem.* **2005**, *58* (2), 82–85. https://doi.org/10.1071/CH04154.

(11) Sievers, M. R.; Armentrout, P. B. Activation of C_2H_6, C_3H_8, and c-C_3H_6 by Gas-Phase Zr^+ and the Thermochemistry of Zr−Ligand Complexes. *Organometallics* **2003**, *22* (13), 2599–2611. https://doi.org/10.1021/om030028u.

(12) Aristov, N.; Armentrout, P. B. Reaction Mechanisms and Thermochemistry of Vanadium Ions with Ethane, Ethene and Ethyne. *J. Am. Chem. Soc.* **1986**, *108* (8), 1806–1819. https://doi.org/10.1021/ja00268a017.

(13) Byrd, G. D.; Burnier, R. C.; Freiser, B. S. Gas-Phase Ion-Molecule Reactions of Fe^+ and Ti^+ with Alkanes. *J. Am. Chem. Soc.* **1982**, *104* (13), 3565–3569. https://doi.org/10.1021/ja00377a004.

(14) Aristov, N.; Armentrout, P. B. Methane Activation by V^+: Electronic and Translational Energy Dependence. *J. Phys. Chem.* **1987**, *91* (24), 6178–6188. https://doi.org/10.1021/j100308a024.

(15) Somorjai, G. A.; Li, Y. *Introduction to Surface Chemistry and Catalysis*; John Wiley & Sons, 2010.

(16) Roithová, J.; Bakker, J. M. Ion Spectroscopy in Methane Activation. *Mass Spectrom. Rev.* **2022**, *41* (4), 513–528. https://doi.org/10.1002/mas.21698.

(17) Schwarz, H. How and Why Do Cluster Size, Charge State, and Ligands Affect the Course of Metal-Mediated Gas-Phase Activation of Methane? *Isr. J. Chem.* **2014**, *54* (10), 1413–1431. https://doi.org/10.1002/ijch.201300134.

(18) Schwarz, H. Chemistry with Methane: Concepts Rather than Recipes. *Angew. Chem. Int. Ed.* **2011**, *50* (43), 10096–10115. https://doi.org/10.1002/anie.201006424.

(19) Shayesteh, A.; Lavrov, V. V.; Koyanagi, G. K.; Bohme, D. K. Reactions of Atomic Cations with Methane: Gas Phase Room-Temperature Kinetics and Periodicities in Reactivity. *J. Phys. Chem. A* **2009**, *113* (19), 5602–5611. https://doi.org/10.1021/jp900671c.
(20) Armentrout, P. B. Methane Activation by 5 d Transition Metals: Energetics, Mechanisms, and Periodic Trends. *Chem. – Eur. J.* **2017**, *23* (1), 10–18. https://doi.org/10.1002/chem.201602015.
(21) Kozubal, J.; Heck, T.; Metz, R. B. Structures of $M^+(CH_4)_n$ (M = Ti, V) Based on Vibrational Spectroscopy and Density Functional Theory. *J. Phys. Chem. A* **2021**, *125* (19), 4143–4151. https://doi.org/10.1021/acs.jpca.1c02217.
(22) van Koppen, P. A. M.; Bowers, M. T.; Haynes, C. L.; Armentrout, P. B. Reactions of Ground-State Ti^+ and V^+ with Propane: Factors That Govern C−H and C−C Bond Cleavage Product Branching Ratios. *J. Am. Chem. Soc.* **1998**, *120* (23), 5704–5712. https://doi.org/10.1021/ja974372s.
(23) Gidden, J.; van Koppen, P. A. M.; Bowers, M. T. Dehydrogenation of Ethene by Ti^+ and V^+: Excited State Effects on the Mechanism for C−H Bond Activation from Kinetic Energy Release Distributions. *J. Am. Chem. Soc.* **1997**, *119* (17), 3935–3941. https://doi.org/10.1021/ja964377+.
(24) Zhang, D.-J.; Feng, D.-C. Theoretical Studies of the Reaction of Vanadium Monocation with Ethane. *Acta Chim. Sin.* **2003**, *61*, 17–21.
(25) Sanders, L.; Hanton, S. D.; Weisshaar, J. C. Electron Spin State Selectivity in Transition Metal Ion Reactions: $V^+(a^3F) + C_2H_6 \rightarrow VC_2H_4^+ + H_2$. *J. Phys. Chem.* **1987**, *91* (20), 5145–5148. https://doi.org/10.1021/j100304a001.
(26) Hanton, S. D.; Sanders, L.; Weisshaar, J. C. Absence of Spin-Orbit Effects on $V^+(a^3F_J) + C_2H_6$ Reaction Cross Section at 0.2 EV. *J. Phys. Chem.* **1989**, *93* (5), 1963–1969. https://doi.org/10.1021/j100342a052.
(27) Sanders, L.; Hanton, S. D.; Weisshaar, J. C. Total Reaction Cross Sections of Electronic State-specified Transition Metal Cations: $V^+ + C_2H_6$, C_3H_8 , and C_2H_4 at 0.2 EV. *J. Chem. Phys.* **1990**, *92* (6), 3498–3518. https://doi.org/10.1063/1.457860.
(28) Ng, C.-Y.; Xu, Y.; Chang, Y.-C.; Wannenmacher, A.; Parziale, M.; Armentrout, P. B. Quantum Electronic Control on Chemical Activation of Methane by Collision with Spin–Orbit State Selected Vanadium Cation. *Phys. Chem. Chem. Phys.* **2021**, *23* (1), 273–286. https://doi.org/10.1039/D0CP04333H.
(29) van Koppen, P. A. M.; Brodbelt-Lustig, J.; Bowers, M. T.; Dearden, D. V.; Beauchamp, J. L.; Fisher, E. R.; Armentrout, P. B. Transition-Metal Ion Mediated Carbon-Hydrogen and Carbon-Carbon Bond Activation of Alkanes: Dynamical Coupling between Entrance and Exit Channel Transition States. *J. Am. Chem. Soc.* **1991**, *113* (7), 2359–2369. https://doi.org/10.1021/ja00007a003.
(30) Metz, R. B. Photofragment Spectroscopy of Covalently Bound Transition Metal Complexes: A Window into C–H and C–C Bond Activation by Transition Metal Ions. *Int. Rev. Phys. Chem.* **2004**, *23* (1), 79–108. https://doi.org/10.1080/01442350310001654065.
(31) Metz, R. B. Spectroscopy of the Potential Energy Surfaces for C-H and C-O Bond Activation by Transition Metal and Metal Oxide Cations. In *Advances in Chemical Physics*; John Wiley & Sons, Ltd, 2008; Vol. 138, pp 331–373. https://doi.org/10.1002/9780470259474.ch6.
(32) Kozubal, J.; Heck, T.; Metz, R. B. Vibrational Spectroscopy of Intermediates and C–H Activation Products of Sequential Zr^+ Reactions with CH_4. *J. Phys. Chem. A* **2020**, *124* (40), 8235–8245. https://doi.org/10.1021/acs.jpca.0c07027.
(33) Kocak, A.; Austein-Miller, G.; Pearson, W. L. I.; Altinay, G.; Metz, R. B. Dissociation Energy and Electronic and Vibrational Spectroscopy of $Co^+(H_2O)$ and Its Isotopomers. *J. Phys. Chem. A* **2013**, *117* (6), 1254–1264. https://doi.org/10.1021/jp305673t.
(34) Kaur, D.; Souza, A. M. de; Wanna, J.; Hammad, S. A.; Mercorelli, L.; Perry, D. S. Multipass Cell for Molecular Beam Absorption Spectroscopy. *Appl. Opt.* **1990**, *29* (1), 119–124. https://doi.org/10.1364/AO.29.000119.

(35) M. J. Frisch; G. W. Trucks; H. B. Schlegel; G. E. Scuseria; M. A. Robb; J. R. Cheeseman; G. Scalmani; V. Barone; B. Mennucci; G. A. Petersson; et al. Gaussian 09, 2013.
(36) Becke, A. D. Density-functional Thermochemistry. III. The Role of Exact Exchange. *J. Chem. Phys.* **1993**, *98* (7), 5648–5652. https://doi.org/10.1063/1.464913.
(37) Grimme, S.; Antony, J.; Ehrlich, S.; Krieg, H. A Consistent and Accurate Ab Initio Parametrization of Density Functional Dispersion Correction (DFT-D) for the 94 Elements H-Pu. *J. Chem. Phys.* **2010**, *132* (15), 154104. https://doi.org/10.1063/1.3382344.
(38) Peverati, R.; Truhlar, D. G. M11-L: A Local Density Functional That Provides Improved Accuracy for Electronic Structure Calculations in Chemistry and Physics. *J. Phys. Chem. Lett.* **2012**, *3* (1), 117–124. https://doi.org/10.1021/jz201525m.
(39) Harrison, J. J.; Allen, N. D. C.; Bernath, P. F. Infrared Absorption Cross Sections for Ethane (C_2H_6) in the 3μm Region. *J. Quant. Spectrosc. Radiat. Transf.* **2010**, *111* (3), 357–363. https://doi.org/10.1016/j.jqsrt.2009.09.010.
(40) Shimanouchi, T. Molecular Vibrational Frequencies. In *NIST Chemistry WebBook, NIST Standard Reference Database Number 69*; Linstrom, P. J., Mallard, W. G., Eds.; National Institute of Standards and Technology: Gaithersburg MD, 1972.
(41) Kocak, A.; Ashraf, M. A.; Metz, R. B. Vibrational Spectroscopy Reveals Varying Structural Motifs in $Cu^+(CH_4)_n$ and $Ag^+(CH_4)_n$ (n = 1–6). *J. Phys. Chem. A* **2015**, *119* (37), 9653–9665. https://doi.org/10.1021/acs.jpca.5b07079.
(42) Hayes, T.; Bellert, D.; Buthelezi, T.; Brucat, P. J. The Bond Length of VAr^+. *Chem. Phys. Lett.* **1998**, *287* (1), 22–28. https://doi.org/10.1016/S0009-2614(98)00129-8.
(43) Lessen, D.; Brucat, P. J. Characterization of Transition Metal–Rare-gas Cations: VAr^+ and VKr^+. *J. Chem. Phys.* **1989**, *91* (8), 4522–4530. https://doi.org/10.1063/1.456790.
(44) Altinay, G.; Metz, R. B. Comparison of IRMPD, Ar-Tagging and IRLAPS for Vibrational Spectroscopy of $Ag^+(CH_3OH)$. *Int. J. Mass Spectrom.* **2010**, *297* (1), 41–45. https://doi.org/10.1016/j.ijms.2010.05.016.
(45) Olney, T. N.; Cann, N. M.; Cooper, G.; Brion, C. E. Absolute Scale Determination for Photoabsorption Spectra and the Calculation of Molecular Properties Using Dipole Sum-Rules. *Chem. Phys.* **1997**, *223* (1), 59–98. https://doi.org/10.1016/S0301-0104(97)00145-6.
(46) Pillai, E. D.; Jaeger, T. D.; Duncan, M. A. IR Spectroscopy and Density Functional Theory of Small $V^+(N_2)_n$ Complexes. *J. Phys. Chem. A* **2005**, *109* (16), 3521–3526. https://doi.org/10.1021/jp050294g.
(47) Adams, C. L.; Schneider, H.; Weber, J. M. Vibrational Autodetachment−Intramolecular Vibrational Relaxation Translated into Electronic Motion. *J. Phys. Chem. A* **2010**, *114* (12), 4017–4030. https://doi.org/10.1021/jp910675n.
(48) Linus Pauling; E. Bright Wilson. *Introduction to Quantum Mechanics With Applications to Chemistry*; Dover Publications: New York, 1985.
(49) Wilson, E. B.; Decius, J. C.; Cross, P. C. *Molecular Vibrations*; Dover Publications: New York, 1980.
(50) Lewis, J. D.; Malloy, T. B.; Chao, T. H.; Laane, J. Periodic Potential Functions for Pseudorotation and Internal Rotation. *J. Mol. Struct.* **1972**, *12* (3), 427–449. https://doi.org/10.1016/0022-2860(72)87050-9.
(51) Moc, J.; Fedorov, D. G.; Gordon, M. S. A Theoretical Study of the Reaction of Ti+ with Ethane. *J. Chem. Phys.* **2000**, *112* (23), 10247–10258. https://doi.org/10.1063/1.481666.
(52) Robertson, W. H.; Price, E. A.; Weber, J. M.; Shin, J.-W.; Weddle, G. H.; Johnson, M. A. Infrared Signatures of a Water Molecule Attached to Triatomic Domains of Molecular Anions: Evolution of the H-Bonding Configuration with Domain Length. *J. Phys. Chem. A* **2003**, *107* (34), 6527–6532. https://doi.org/10.1021/jp030474v.
(53) Carnegie, P. D.; McCoy, A. B.; Duncan, M. A. IR Spectroscopy and Theory of $Cu^+(H_2O)Ar_2$ and $Cu^+(D_2O)Ar_2$ in the O−H (O−D) Stretching Region: Fundamentals and Combination Bands. *J. Phys. Chem. A* **2009**, *113* (17), 4849–4854. https://doi.org/10.1021/jp901231q.

(54) Bhattacharya, I.; Banerjee, P.; Sadhukhan, J.; Chakraborty, T. Modulations of *ν*O–H and *ν*C═O Stretching Frequencies of Difluoroacetic Acid with Internal Rotation of CHF_2 Rotor: A Combined Vapor Phase and Matrix Isolation Infrared Spectroscopy Study. *J. Phys. Chem. A* **2019**, *123* (13), 2771–2779. https://doi.org/10.1021/acs.jpca.8b12528.
(55) Moore, C. E. *Atomic Energy Levels As Derived From the Analyses of Optical Spectra*; Circular of the National Bureau of Standards; United States National Bureau of Standards: Washington, DC, 1949; Vol. 1.
(56) Wang, J.; Mbah, C. F.; Przybilla, T.; Apeleo Zubiri, B.; Spiecker, E.; Engel, M.; Vogel, N. Magic Number Colloidal Clusters as Minimum Free Energy Structures. *Nat. Commun.* **2018**, *9* (1), 5259. https://doi.org/10.1038/s41467-018-07600-4.
(57) Zhang, D.; Fu, X.; Wang, R.; Liu, C. Theoretical Study of the Reaction of Titanium Ion with Ethane: Structure, Mechanism, and Potential Energy Surface. *Can. J. Chem.* **2005**, *83* (5), 485–492. https://doi.org/10.1139/v05-076.

Tables and Figures

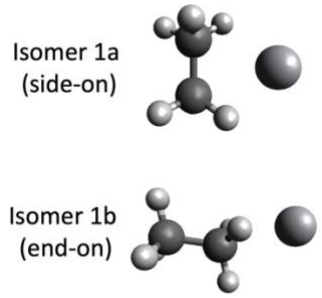

Figure 1. Structures of the two major isomer classes for $V^+(C_2H_6)$. Note that, while both isomers have a nominal denticity of η^2, determining the actual denticity of the side-on isomer is not straightforward, as discussed in the text.

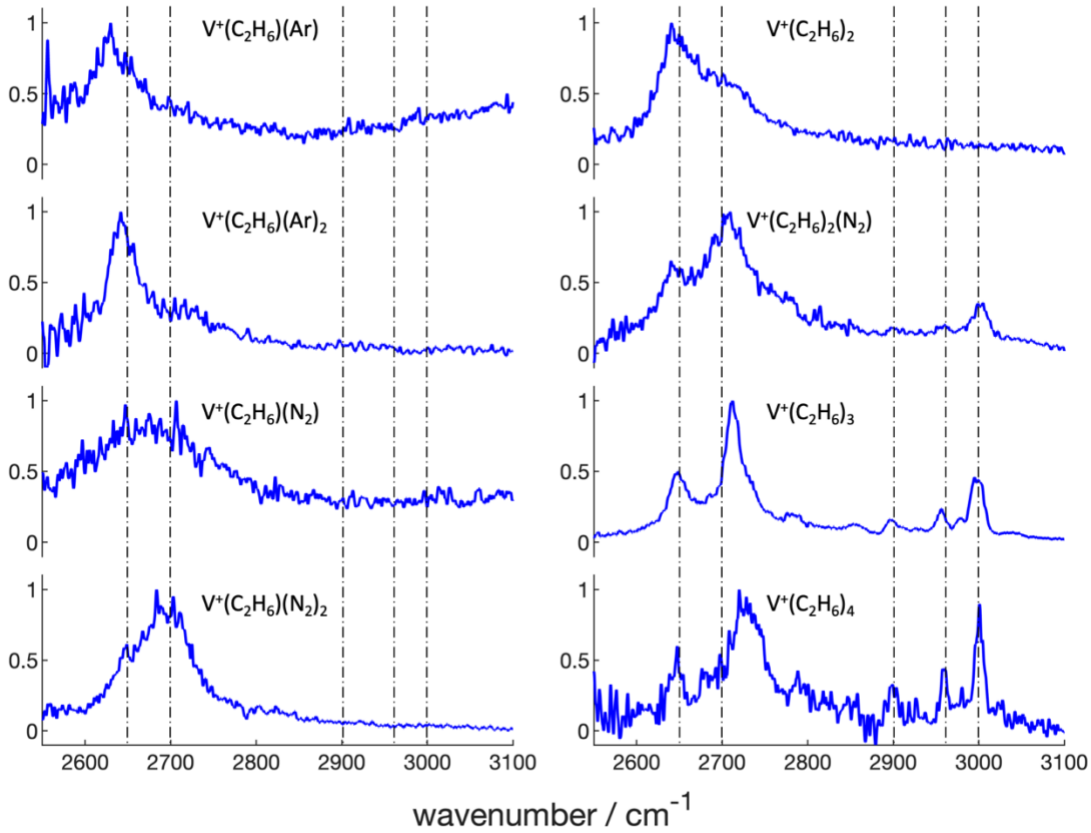

Figure 2. Photodissociation spectra for $V^+(C_2H_6)$, each obtained using a different tagging method (left), and for vanadium-ethane clusters with more than one ethane (right). Vertical lines are included at 2650, 2700, 2900, 2960, and 3000 cm^{-1} to help visualize shifts to spectral features.

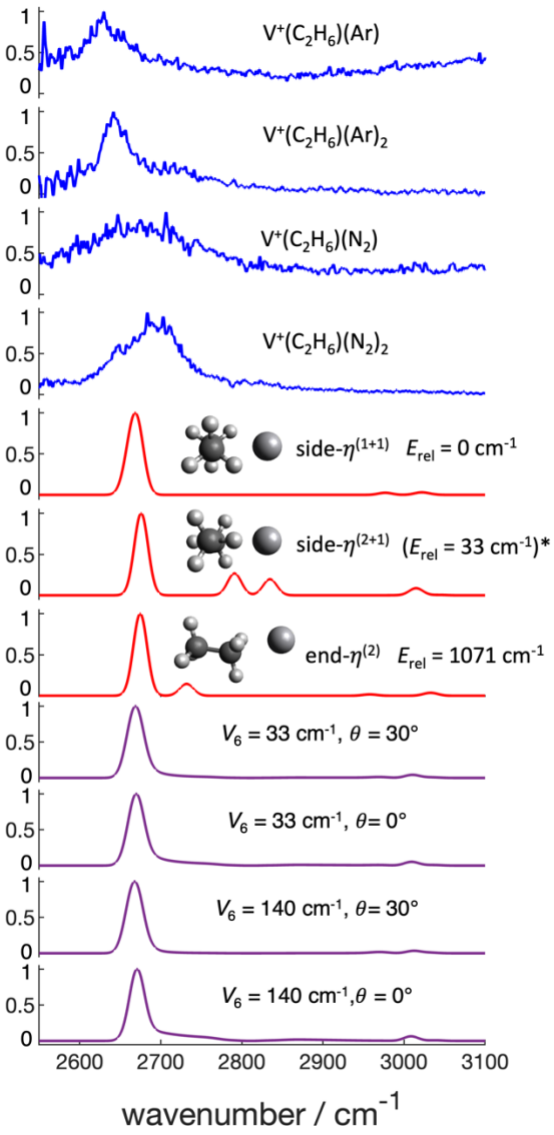

Figure 3. Photodissociation spectra for $V^+(C_2H_6)$ clusters including experimental spectra (blue), simulated spectra from scaled harmonic frequency calculations (B3LYP/6-311++G(3df,3pd)) of the main untagged isomer classes (red), and simulated spectra of side-on isomers incorporating hindered-rotor analysis (purple). *Note that the side-on $\eta^{(2+1)}$ configuration is not predicted to be a minimum at this level of theory, but is an important part of our hindered-rotor analysis. The value of E_{rel} = 33 cm^{-1} refers to vibrationally adiabatic barrier height calculated by including zero-point energy for all modes except for the hindered rotor motion of ethane. The values accompanying the hindered-rotor simulated spectra indicate PES parameters (see SI for more information). The extreme similarity between the hindered-rotor simulated spectra highlights that all rotational angles are important, regardless of the finer structural details of the PES.

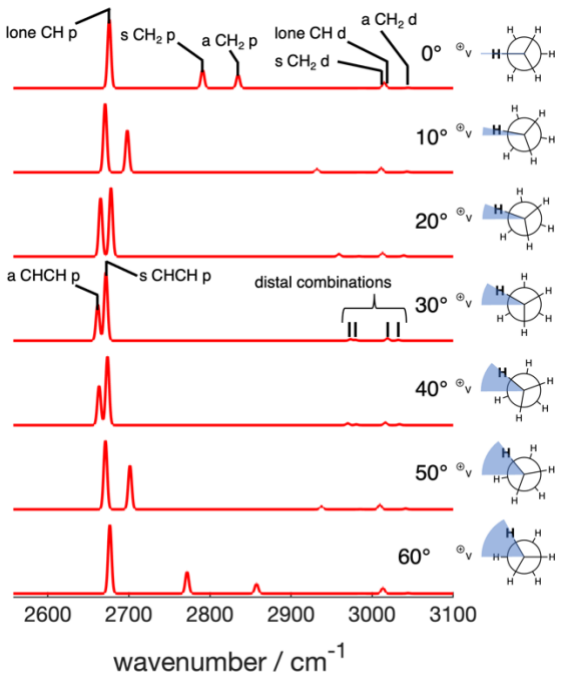

Figure 4. Scaled harmonic frequency spectra for the C-H stretching region at representative HCCV dihedral angles for $V^+(C_2H_6)$ in a side-on configuration (B3LYP/6-311++G(3df,3pd)). Gaussian broadening is performed with a resolution of 5 cm^{-1} to distinguish underlying spectral features. Individual peaks for the two most symmetric conformations are assigned as proximate (p), distal (d), symmetric (s), anti-symmetric (a), and lone.

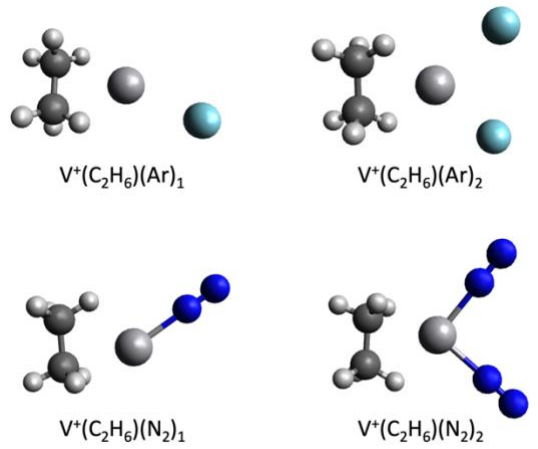

Figure 5. Lowest-energy isomers for tagged $V^+(C_2H_6)$ calculated using B3LYP/6-311++G(3df,3pd).

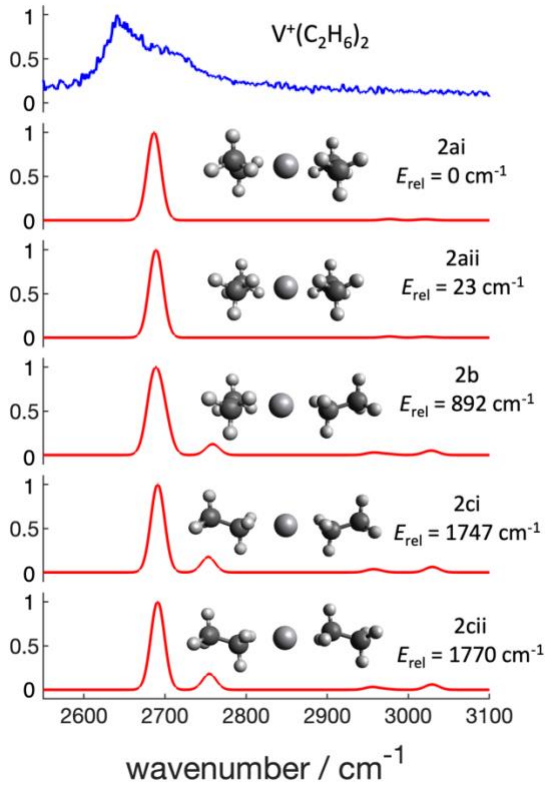

Figure 6. Photodissociation spectra of untagged $V^+(C_2H_6)_2$, including simulated scaled harmonic frequency spectra and structures of the lowest-energy isomer classes (B3LYP/6-311++G(3df,3pd)).

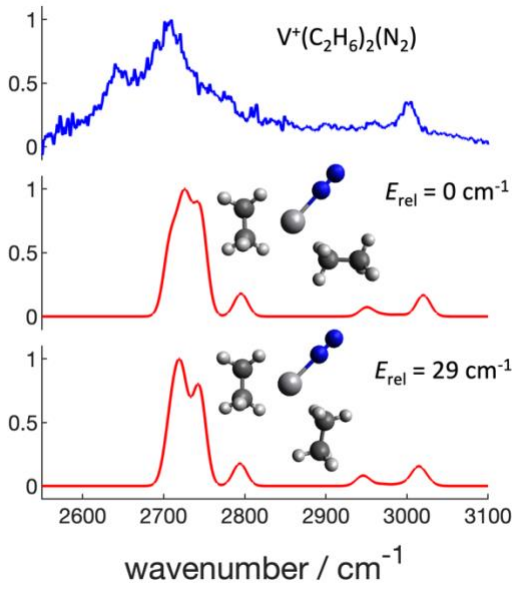

Figure 7. Photodissociation spectrum of the nitrogen-tagged species $V^+(C_2H_6)_2(N_2)$, including simulated scaled harmonic frequency spectra and structures for the lowest-energy isomer class (B3LYP/6-311++G(3df,3pd)).

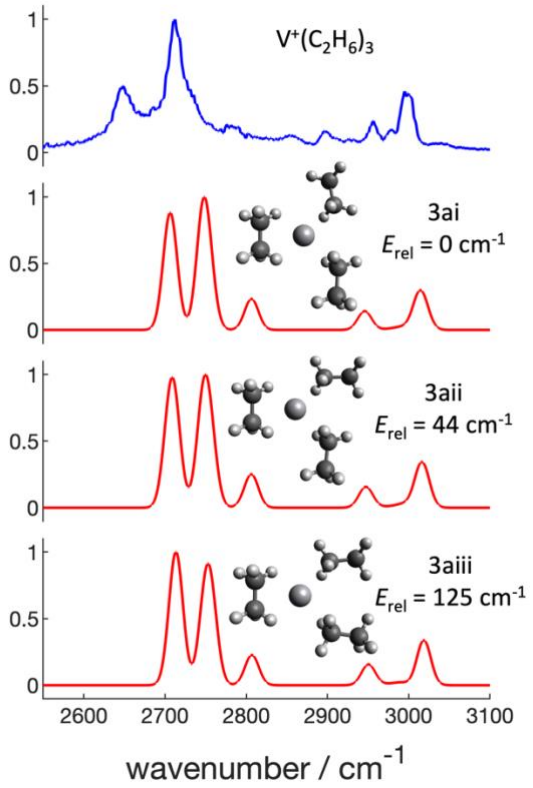

Figure 8. Photodissociation spectrum of $V^+(C_2H_6)_3$, including simulated spectra and isomers (B3LYP/6-311++G(3df,3pd)).

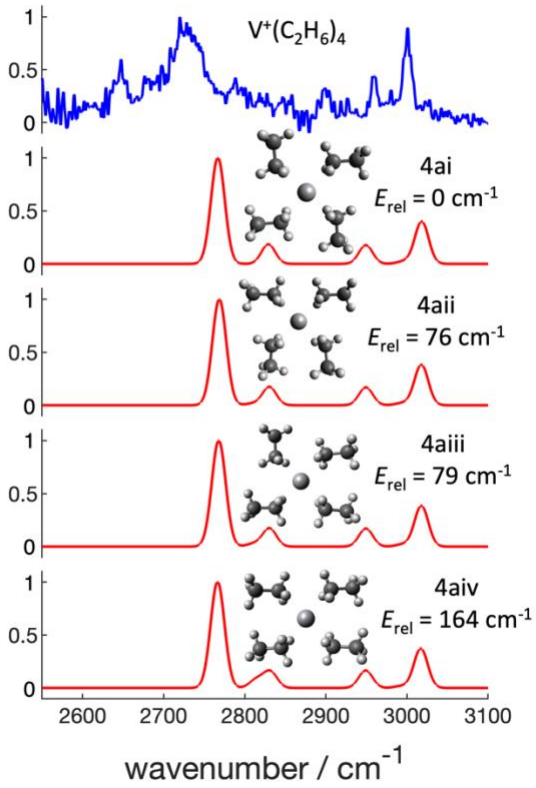

Figure 9. Photodissociation spectrum of $V^+(C_2H_6)_4$, including simulated spectra and isomers (B3LYP/6-311++G(3df,3pd)).

Table 1. Calculated binding and relative isomer energies, including zero-point energy, for $V^+(C_2H_6)_n$ clusters included in our study. Although all isomer classes are represented, the list of isomers in each class is not exhaustive. Energies are given both with respect to the lowest-energy isomer of a given cluster size (ΔE_{isomer}) and with respect to cluster dissociation into free V^+ and ethane (ΔE_{total}). For each isomer geometry, ethane molecules in a side-on configuration are designated "s" and those in an end-on configuration are designated "e". The notation for denticity is described in the text. *Note that Isomer 1aii is not predicted to be a minimum on the B3LYP/6-311++G(3df,3pd) surface due to the possibility of ethane rotor motion, as described in the text.

isomer	geometry	symmetry	ΔE_{isomer} / cm^{-1}	ΔE_{total} / cm^{-1}
1ai	s-$\eta^{(1+1)}$	C_2	0	-7760
1aii*	s-$\eta^{(2+1)}$	C_s	33*	-7727
1bi	e-η^2	C_s	1071	-6689
1bii	e-η^2	C_s	1293	-6467
2ai	s-$\eta^{(1+1)}$, s-$\eta^{(1+1)}$	D_2	0	-14375
2aii	s-$\eta^{(1+1)}$, s-$\eta^{(1+1)}$	C_{2h}	23	-14352
2b	s-$\eta^{(1+1)}$, e-η^2	C_1	892	-13483
2ci	e-η^2, e-η^2	C_{2v}	1747	-12628
2cii	e-η^2, e-η^2	C_{2h}	1770	-12605
3ai	s-$\eta^{(1+1)}$, e-η^2, e-η^2	C_2	0	-16290
3aii	s-$\eta^{(1+1)}$, e-η^2, e-η^2	C_1	44	-16246
3aiii	s-$\eta^{(1+1)}$, e-η^2, e-η^2	C_2	125	-16165
3b	e-η^2, e-η^2, e-η^2	C_1	958	-15331
3ci	s-$\eta^{(1+1)}$, s-$\eta^{(1+1)}$, e-η^1	C_1	1476	-14814
3cii	s-$\eta^{(1+1)}$, s-$\eta^{(1+1)}$, e-η^1	C_1	1487	-14803
3ciii	s-$\eta^{(1+1)}$, s-$\eta^{(1+1)}$, e-η^1	C_1	1501	-14788
4ai	e-η^2, e-η^2, e-η^2, e-η^2	C_{4h}	0	-17939
4aii	e-η^2, e-η^2, e-η^2, e-η^2	C_2	76	-17863
4aiii	e-η^2, e-η^2, e-η^2, e-η^2	C_1	79	-17860
4aiv	e-η^2, e-η^2, e-η^2, e-η^2	D_2	164	-17774
4bi	s-$\eta^{(1+1)}$, e-η^2, e-η^2, e-η^1	C_1	1353	-16585
4bii	s-$\eta^{(1+1)}$, e-η^2, e-η^2, e-η^1	C_1	1399	-16540
4biii	s-$\eta^{(1+1)}$, e-η^2, e-η^2, e-η^1	C_1	1483	-16455
4c	s-$\eta^{(1+1)}$, s-$\eta^{(1+1)}$, e-η^1, e-η^1	C_1	2795	-15144
5a	e-η^2, e-η^2, e-η^2, e-η^2, e-η^1	C_1	0	-18173
6a	e-η^2, e-η^2, e-η^2, e-η^2, e-η^1, e-η^1	C_1	0	-18347

Graphic For Table of Contents Only